ARL-TR-8092 ● AUG 2017

US Army Research Laboratory

ALEGRA-MHD Simulations for Magnetization of an Ellipsoidal Inclusion

by Michael Grinfeld and John Niederhaus

NOTICES

Disclaimers

The findings in this report are not to be construed as an official Department of the Army position unless so designated by other authorized documents.

Citation of manufacturer's or trade names does not constitute an official endorsement or approval of the use thereof.

Destroy this report when it is no longer needed. Do not return it to the originator.

ARL-TR-8092 ● AUG 2017

US Army Research Laboratory

ALEGRA-MHD Simulations for Magnetization of an Ellipsoidal Inclusion

by Michael Grinfeld
Weapons and Materials Research Directorate (ARL)

by John Niederhaus
Sandia National Laboratories, Albuquerque, NM

REPORT DOCUMENTATION PAGE

Form Approved
OMB No. 0704-0188

1. REPORT DATE *(DD-MM-YYYY)*	2. REPORT TYPE	3. DATES COVERED (From - To)
August 2017	Technical Report	June 2016–June 2017

4. TITLE AND SUBTITLE
ALEGRA-MHD Simulations for Magnetization of an Ellipsoidal Inclusion

5a. CONTRACT NUMBER

5b. GRANT NUMBER

5c. PROGRAM ELEMENT NUMBER

6. AUTHOR(S)
Michael Grinfeld and John Niederhaus

5d. PROJECT NUMBER

5e. TASK NUMBER

5f. WORK UNIT NUMBER

7. PERFORMING ORGANIZATION NAME(S) AND ADDRESS(ES)
US Army Research Laboratory
ATTN: RDRL-WMP-C
Aberdeen Proving Ground, MD 21005-5069

8. PERFORMING ORGANIZATION REPORT NUMBER
ARL-TR-8092

9. SPONSORING/MONITORING AGENCY NAME(S) AND ADDRESS(ES)

10. SPONSOR/MONITOR'S ACRONYM(S)

11. SPONSOR/MONITOR'S REPORT NUMBER(S)

12. DISTRIBUTION/AVAILABILITY STATEMENT
Approved for public release; distribution is unlimited.

13. SUPPLEMENTARY NOTES
Sandia National Laboratories is a multimission laboratory managed and operated by National Technology and Engineering Solutions of Sandia, LLC., a wholly owned subsidiary of Honeywell International, Inc., for the US Department of Energy's National Nuclear Security Administration under contract DE-NA0003525.

14. ABSTRACT

Here we verify how reliable the ALEGRA MHD code is in its static limit. We explore in the quasi-static approximation the process of evolution of the magnetic fields inside and outside an inclusion. A simple closed-form analytic solution similar to the Eshelby theory is derived for magnetic induction in an ellipsoidal inclusion of magnetically permeable material after magnetic diffusion has saturated. The simplicity of the interior solution lends itself well to verification of computational electromagnetic simulations. Convergence testing under spatial mesh refinement using this exact solution shows that the equilibrium magnetized state can be reached by transient means via computation with ALEGRA. The computed solution in the interior core of the ellipsoid converges to the exact solution at first order, as expected, for a very large range of spatial mesh sizes spanning the very coarsest to the very finest meshes that can be used. The error in the computed solution is dominated by the interfacial region where mixed-material elements are present. When the interfacial region is included, the error magnitudes are larger by more than an order of magnitude, and the convergence rate drops from roughly 1 to roughly 0.5. These issues appear to be associated with the enforcement of natural interface conditions and the element-level homogenization scheme for mixed-material elements.

15. SUBJECT TERMS
magnetic diffusion, permeability, computational electromagnetism, verification, magnetohydrodynamics

16. SECURITY CLASSIFICATION OF:			17. LIMITATION OF ABSTRACT	18. NUMBER OF PAGES	19a. NAME OF RESPONSIBLE PERSON
a. REPORT	b. ABSTRACT	c. THIS PAGE			Michael Grinfeld
Unclassified	Unclassified	Unclassified	UU	26	19b. TELEPHONE NUMBER (Include area code) 410-278-7030

Contents

List of Figures iv

List of Tables iv

Acknowledgments v

1. Introduction and Theory 1

1.1 MHD Master System 1

1.2 Exact Solution for an Ellipsoidal Inclusion 2

1.3 Geometric Tensor 5

1.4 Closed-Form Solution 7

2. Numerical Model and Simulations 8

2.1 The ALEGRA-MHD Code 8

2.2 Verification Strategy 9

2.3 Sample Simulation Results 10

2.4 Verification Analysis 11

2.5 Origin of Diminished Convergence Rates 13

2.6 Computational Cost 15

3. Conclusions 15

4. References 16

List of Symbols, Abbreviations, and Acronyms 17

Distribution List 18

List of Figures

Fig. 1 Computed solutions for the vertical magnetic induction ($\boldsymbol{By}$) from ALEGRA during and after equilibration. The analytic solution predicts 1.5788 T inside the ellipsoid. 10

Fig. 2 Geometry for verification test in ALEGRA (not to scale) 11

Fig. 3 Convergence behavior with and without the layer of mixed elements on the ellipsoid surface 12

Fig. 4 Convergence trends for (*a*) the *x*-component and (*b*) the *y*-component of magnetic induction, for various subregions of the spheroid inclusion 13

Fig. 5 Spatial distribution of error in ellipsoid-interior magnetic induction at steady state, arranged by increasing number of *N* elements spanning the axial length of the ellipsoid 14

List of Tables

Table 1 Convergence rates for spheroid verification study for various subregions. 13

Acknowledgments

Special thanks to Dr James Carleton (Sandia National Laboratories) for several helpful discussions regarding aspects of the Eshelby theory and the related mathematics, and to Dr Robert Doney (US Army Research Laboratory) and the Department of Defense High Performance Computing Modernization Program for providing access to computational resources for these simulations.

INTENTIONALLY LEFT BLANK.

1. Introduction and Theory

ALEGRA is a finite-element multiphysics code designed for modeling shock hydrodynamics and coupled electromagnetic phenomena including magnetohydrodynamics (MHD). This multiphysics capability is a key feature of ALEGRA and the result of many years of multidisciplinary effort. Verification and validation (V&V) of ALEGRA is also a significant undertaking. Fortunately, the proper compartmentalization is ingrained in the architecture of ALEGRA. In other words, various modules of ALEGRA can be used without others when necessary. Therefore, the V&V procedures can be compartmentalized as well.

We have 2 goals in pursuing this project. First, we explore in the quasi-static approximation the evolution of the magnetic fields inside and outside an inclusion and the parameters for which the quasi-static approach provides for self-consistent results. Second, we explore how reliable ALEGRA is in its static limit, specifically for magnetic diffusion. By the static limit we understand the stationary states without macroscopic current. We choose quite a general class of 3-D solutions for which a linear isotropic metallic matrix is placed inside a stationary magnetic field approaching a constant value at infinity.

Analysis for related magnetic diffusion problems appears throughout the literature. Knoepfel[1] considered linear and nonlinear magnetic diffusion for simple geometries and nonpermeable materials. Rieben and White[2] performed simulations for linear transient magnetic diffusion in several geometries, including annular and spherical shapes. Woodson and Melcher[3] analyzed permeable materials for a slab geometry. Brauer[4] considered slabs and cylinders with linear and nonlinear permeability and finite-element modeling. Here we consider linear permeability with an ellipsoidal geometry in 3-D. This expands upon the previous work described in Refs. 5 and 6, which examine 2-D magnetic diffusion into an elliptic cylinder. The 3-D ellipsoidal situation is considerably more challenging because of the size of the simulations required to resolve the inclusion.

1.1 MHD Master System

The analysis of quasi-statics is based on the following reduced Maxwell system:

$$z^{ijk}\nabla_j E_k = -\frac{1}{c}\frac{\partial B^i}{\partial t}, \qquad z^{ijk}\nabla_j H_k = \frac{4\pi}{c}J^i. \tag{1}$$

These bulk partial differential equations (PDEs) should be augmented with 1) the constitutive equations $J^i = \sigma^{ij}E_j$ (Ohm's law), 2) the constitutive equation $B^i = B^i(H^k)$, 3) boundary conditions $\left[B^i\right]^+_- n_i = 0$, $\left[H^i\right]^+_- \tau_i = 0$, 4) the conditions at infinity, and 5) appropriate conditions at infinity as well as with corresponding initial conditions.

Here, z^{ijk} is the covariant Levi-Civita skew-symmetric tensor; E_i, H_i, and B_i are the electric and magnetic field and magnetic induction, respectively; J_i is the electric current density of free charges, c is the speed of light in vacuum, and σ_{ij} is electrical conductivity. In the boundary conditions, n_i and τ_i are the normal and tangent vectors to the discontinuity boundaries. The ALEGRA code uses the vector potential A_i. The vectors A_i and H_i are interconnected by the covariant differential relation $H^i = z^{ijk}\nabla_j A_k$.

1.2 Exact Solution for an Ellipsoidal Inclusion

There are few exact 2-D and 3-D solutions on the MHD master system. For the static equilibrium configuration, a closed-form solution can be obtained for an ellipsoidal inclusion in an infinite isotropic matrix, in particular, in vacuum, which allows generalization for anisotropic and nonlinear media.[7–9] Its origin traces back to the pioneering papers by Eshelby.[10,11] This solution is described in the following paragraphs and used in our project for verification purposes.

Consider an ellipsoid with the semi-axes a_1, a_2, and a_3 coinciding with the Cartesian axes z^1, z^2, and z^3. We assume that the ellipsoidal domain is filled with a linear isotropic substance with magnetic permeability μ. We then assume that the ellipsoid is immersed in the unbounded space in which there is a uniform magnetic field $H^{i\circ}$.

If there is an ellipsoidal inclusion, the otherwise uniform field $H^i = H^{i\circ}$ will change. The changes are particularly strong inside the ellipse and in its vicinity. At infinity, the newly generated field H^i approaches its original value $H^{i\circ}$.

For the time-independent fields and in the absence of macroscopic currents J^i, the system (Eq. 1) splits into 2: one for the electrostatic field and the other for the magnetic field

$$z^{ijk}\nabla_j H_k = 0\,, \tag{2}$$

with these normal and tangential boundary conditions at the surface of the inclusion:

$$\left[\mu H^i\right]^+_- n_i = 0, \qquad \left[H^i\right]^+_- \tau_i = 0. \tag{3}$$

The initial conditions become unnecessary in this case. Let $H^{i\circ} = B^{i\circ}$ be the uniform magnetic field in vacuum occupying the whole space. Consider a magneto-sensitive body ω immersed in a uniform field. When the body is introduced, the magnetic field $H^{i\circ}$ and induction $B^{i\circ}$ change, both inside and outside the inclusion. If the inclusion is finite in size, then the outside field $H^i = B^i$ in the vacuum only asymptotically approaches the uniform fields $H^{i\circ} = B^{i\circ}$ at $z^i \to \infty$:

$$H^i_{|z|\to\infty} = B^i_{|z|\to\infty} \;\; \to \;\; H^{i\circ} = B^{i\circ}, \tag{4}$$

where z^i are the spatial coordinates. The disturbance $(H^i - H^{i\circ})$ will be generated because of the dipole magnetization M^i appearing inside the inclusion, but whose influence will be sensed both inside and outside the inclusion.

This problem for an ellipsoidal inclusion in unbounded space has been analyzed by many outstanding mathematicians and physicists. First, the problem was considered in the contexts of gravitation and cosmology. Later on, the problem and its solutions found multiple applications in many other disciplines, including electromagnetism, and it is in this context that we use it here.

We seek solutions assuming that H_i is a potential field, that is,

$$H_i = -\nabla_i \eta \ , \tag{5}$$

where $\eta(z)$ is a scalar potential field that should not be confused with the scalar potential of the electrostatic field, or with the vector potential A^i of the magnetic field. When dealing with an ellipsoid immersed in the uniform field $H_i = H_i{}^\circ$ at infinity, we will be looking for a solution $\eta_-(z)$ inside the ellipsoid in the following form:

$$\eta_-(z) = -K_i z^i \ , \tag{6}$$

which automatically satisfies the PDE in Eq. 2 and implies that $H_i = K_i$ inside the ellipsoid.

For the solution outside the ellipsoidal inclusion, we will be seeking an expression of the form

$$\eta_+(z) = S^i \nabla_i \Theta_+ - H_i{}^\circ z^i \ , \tag{7}$$

where Θ is the Newtonian potential of the ellipsoid, given by the relationship

$$\Theta(z) = \int_\omega \frac{d\omega^*}{|z - z^*|} \tag{8}$$

and it satisfies the PDEs:

$$\nabla_i \nabla^i \Theta = -4\pi \qquad \text{Inside the ellipsoid.}$$

$$\nabla_i \nabla^i \Theta = 0 \qquad \text{Outside the ellipsoid.} \tag{9}$$

Solutions of this form automatically satisfy the PDE in Eq. 2 and the condition at infinity

$$H_i(z) \to H_i^\circ \text{ at } |z| \to \infty\,, \tag{10}$$

and it is implied that the following expression holds outside the ellipsoid:

$$H_i = H_i^\circ - G_i^j \nabla_j \Theta\,, \tag{11}$$

where G_i^j is a uniform tensor to be determined.

As is well-known,[12] the Newtonian potential within the ellipsoid is described by the quadratic form

$$\Theta_-(z) = C - \frac{1}{2} Y_{ij} z^i z^j, \tag{12}$$

where C is a constant and Y_{ij} is a symmetric tensor. Y_{ij} depends only on the geometry of the ellipsoid—we call it the "geometric tensor". It is described in Section 1.3. Thus, to find an exact solution for H_i, we need to find the constant C and the 2 unknown vectors K_i (interior) and S_i (exterior).

The potential $\Theta_+(z)$ outside the ellipsoid is much more complex. Fortunately, if the potential inside the inclusion is known (i.e., the constants C and Y_{ij} are known), then we can uniquely recover the potential outside the inclusion. Using the boundary conditions in Eq. 3, we can find all of the constants.

Using the potential-based definition of H_i in Eq. 5, we can rewrite the surface tangential and normal boundary conditions in Eq. 3 as follows:

$$\eta_- = \eta_+ \qquad \text{(tangential component)} \tag{13}$$

and

$$\mu_- \nabla_i \eta_- n^i = \nabla_i \eta_+ n^i \qquad \text{(normal component)}\,. \tag{14}$$

Then, with the help of Eqs. 6 and 7, we get

$$K_i z^i = -S^k \nabla_k \Theta_+ + H_i^\circ z^i \tag{15}$$

and

$$\mu_{-} K_i n^i = \left(-S^k \nabla_i \nabla_k \Theta_{+} + H_i^{\circ}\right) n^i \, . \tag{16}$$

First derivatives of the potential Θ remain continuous across the ellipsoid surface. Therefore, we can rewrite the surface tangential boundary condition in Eq. 15 as

$$K_i - Y_{ki} S^k = H_i^{\circ} \, . \tag{17}$$

Similarly, we can rewrite the pointwise surface normal boundary condition in Eq. 16 as the following algebraic condition:

$$\mu_{-} K_i + S^k (4\pi \delta_{ik} - Y_{ik}) = H_i^{\circ} \, , \tag{18}$$

where δ_{ik} is the Kronecker delta tensor. Using Eq.17, we can rewrite Eq. 18 as

$$(\mu_{-} - 1) K_i + 4\pi S_i = 0 \, . \tag{19}$$

To summarize, Eqs. 17 and 19 comprise a system of 2 linear vector equations with 2 unknown vectors K_i and S_i. Eliminating S_i from the system yields

$$\left(\delta_{ki} + Y_{ki} \frac{\mu_{-} - 1}{4\pi}\right) K^k = H_i^{\circ}. \tag{20}$$

After solving Eq. 20 with respect to K^k, we can find S_i from the equation

$$S_i = \frac{\mu_{-} - 1}{4\pi} K_i. \tag{21}$$

Since we have thus found the vectors K_i and S_i, the determination of the exact solution is complete, and all that remains is to work out closed-form solutions for H_i, which can be used in verification studies for ALEGRA.

1.3 Geometric Tensor

To build closed-form solutions, first the geometric tensor Y_{ij} must be determined. The main components of Y_{ij} for an ellipsoid with semi-axes equal to a_i are given by the formulae

$$Y_{ii} = 2\pi a_1 a_2 a_3 \int_0^{\infty} \frac{dq}{(a_i^2 + q)\sqrt{(a_1^2 + q)(a_2^2 + q)(a_3^2 + q)}} \tag{22}$$

and the constant C appearing in Eq. 12 is given by

$$C = a_1 a_2 a_3 \int_0^\infty \frac{dq}{\sqrt{(a_1^2+q)(a_2^2+q)(a_3^2+q)}} . \qquad (23)$$

Here, we simplify the problem by limiting our interest to an ellipsoidal inclusion that has 2 planes of symmetry—that is, it has 2 axes equal in length, in which case it is a spheroid. In the case of a spheroid with semi-axes $a_1 = a_2 = M$ and $a_3 = N$, we get

$$Y_{11} = Y_{22} = 2\pi M^2 N \int_0^\infty \frac{dq}{(M^2+q)\sqrt{N^2+q}} \quad \text{and}$$

$$Y_{33} = 4\pi - 2Y_{11} \qquad (24)$$

The integral in Eq. 22 can be evaluated using elliptic integrals. For a spheroidal shape, the elliptic integrals reduce to the more elementary trigonometric functions. Defining a spheroid aspect ratio $e = N/M$, we can generate expressions for oblate ($e \leq 1$) and elongated ($e \geq 1$) spheroids. For the oblate (saucer-like) case with the axis oriented in the 3-direction, we get

$$Y_{11} = Y_{22} = 2\pi \frac{e}{(1-e^2)^{3/2}} \left(\arccos e - e\sqrt{1-e^2} \right) \quad \text{and}$$

$$Y_{33} = 4\pi - 2Y_{11}, \quad e \leq 1 . \qquad (25)$$

For the prolate or "elongated" (cigar-like) case with the axis oriented in the 1-direction, we get

$$Y_{22} = Y_{33} = 2\pi \frac{e}{(e^2-1)^{3/2}} \left(e\sqrt{e^2-1} - \arccos e \right) \quad \text{and}$$

$$Y_{11} = 4\pi - 2Y_{22}, \quad e \geq 1 . \qquad (26)$$

The geometric tensor can be written more generally for a spheroid as

$$Y_{ki} = Y_{axial} l_k l_i + \left(2\pi - \tfrac{1}{2} Y_{axial} \right) (\delta_{ki} - l_k l_i) , \qquad (27)$$

where the unit vector l_i is aligned with the spheroid axis, and Y_{axial} is given by Y_{33} in Eq. 25 for the oblate case, and by Y_{11} in Eq. 26 for the prolate case. The off-diagonal components of the geometric tensor are zero by the assumed alignment of the spheroid to the 1, 2, 3 axes.

1.4 Closed-Form Solution

To work out a closed-form solution for the field in the ellipsoid interior, we first solve Eq. 20 for K_i. Component-wise, this yields

$$\underline{i=1}$$

$$\sum_{k=1}^{3}\left(\delta_{k1}K^k + Y_{k1}\frac{\mu_- - 1}{4\pi}K^k\right) = H_1{}^\circ$$

$$K^1\left(1 + Y_{11}\frac{\mu_- - 1}{4\pi}\right) = H_1{}^\circ\,. \tag{28}$$

$$\underline{i=2}$$

$$\sum_{k=1}^{3}\left(\delta_{k2}K^k + Y_{k2}\frac{\mu_- - 1}{4\pi}K^k\right) = H_2{}^\circ$$

$$K^2\left(1 + Y_{22}\frac{\mu_- - 1}{4\pi}\right) = H_2{}^\circ\ . \tag{29}$$

$$\underline{i=2}$$

$$\sum_{k=1}^{3}\left(\delta_{k3}K^k + Y_{k3}\frac{\mu_- - 1}{4\pi}K^k\right) = H_3{}^\circ$$

$$K^3\left(1 + Y_{33}\frac{\mu_- - 1}{4\pi}\right) = H_3{}^\circ\ . \tag{30}$$

Simplifying these expressions, we have

$$K^i = H^{i\circ}\left(1 + \frac{\mu_- - 1}{4\pi}Y_{II}\right)^{-1}\,, \tag{31}$$

where the subscript *II* notation indicates diagonal components rather than summation over repeated indices.

Having found K_i, we can write an expression for the field in the ellipsoid interior. To obtain the exterior solution, we must also substitute K_i into Eq. 21, as follows:

$$S_i = H_i{}^\circ\left(\frac{\mu_- - 1}{4\pi}\right)\left(1 + \frac{\mu_- - 1}{4\pi}Y_{II}\right)^{-1}\,. \tag{32}$$

However, the form of the potential Θ_+outside the ellipsoid is not analytically simple. Thus, even having found S_i, it will not be straightforward to comprehend the behavior of H_i outside the ellipsoid. At this point, we proceed by limiting the scope of our study to the ellipsoid interior.

The ellipsoid interior has a relatively simple solution, which is found by combining Eqs. 5 and 6 and to yield $H_i = K_i$, or, from Eq. 31,

$$H^i = H^{i\circ}\left(1 + \frac{\mu_- - 1}{4\pi} Y_{II}\right)^{-1} . \tag{33}$$

Extending this to the magnetic induction and retaining the assumed orientation of the ellipsoid axis along the 1-direction, we have

$$B^i = \mu_- H^{i\circ}\left(1 + \frac{\mu_- - 1}{4\pi} Y_{II}\right)^{-1} . \tag{34}$$

Together with the definitions of the geometric tensor Y_{II} in Eqs. 25 and 26 for the oblate and prolate spheroids, we have a simple closed-form solution for the magnetic induction interior to the spheroid, which lends itself well to verification of computational electromagnetics simulations. This represents the magnetic induction remaining in the material after magnetic diffusion has saturated and currents have decayed to zero, leaving the steady-state "equilibrium" configuration of the field. This field is uniform within the ellipsoid and depends only on the geometry of the ellipsoid, its relative permeability, and the imposed field at infinity.

2. Numerical Model and Simulations

Having now arrived at a transparent closed-form solution for the magnetic field at equilibrium inside an ellipsoidal inclusion, we can use it as a verification tool for numerical modeling. Transient magnetic diffusion calculations can be performed using the ALEGRA-MHD code,[13] and the accuracy of these calculations can be probed.

2.1 The ALEGRA-MHD Code

The "transient magnetics" module of the ALEGRA-MHD code (henceforward ALEGRA) computes solutions to the reduced Maxwell system of Eq. 1 in quasi-static fashion. It is assumed the medium is stationary, with an electrical conductivity σ and a magnetic permeability μ that are fixed for each material. The system is recast in terms of the vector potential A_i and transformed to SI units, and

appropriate constitutive relationships are incorporated. These include Ohm's law $J^i = \sigma E^i$ and a simple linear relationship between the magnetic field and the magnetic induction, $B^i = \mu H^i$. An implicit linear solver is used with a finite-element discretization to evolve the solution forward in time.

ALEGRA is equipped to handle a much broader class of problems, including high-strain-rate deformation, mechanical and electromagnetic forces, and Ohmic heating. These are encompassed within ALEGRA's broader MHD capability. In these systems, body-fitted meshes and purely Lagrangian approaches are usually impractical because of large strains that are encountered. Therefore, ALEGRA includes a 2-step Lagrange-remap formulation that permits material motion across the mesh, and the presence of multiple materials in a single element. For the present work, only the transient magnetics module is considered—that is, ALEGRA's capability to simulate the evolution of magnetic fields in a domain containing stationary materials of differing conductivity and permeability. But connections to the broader class of problems are retained by using a regular Eulerian mesh, as would be used in those situations, with material interfaces only resolved in volumetrically mixed multimaterial elements. This facilitates investigation into whether transient magnetics problems can be accurately represented in this way. Considering only Eulerian meshes, however, poses a significant obstacle, since material interfaces are not resolved explicitly. Here we examine the impact of the Eulerian approximation.

2.2 Verification Strategy

The equilibrium solution for the ellipsoid problem described previously is obtained in ALEGRA in quasi-static fashion by a series of implicitly integrated timesteps capturing the time evolution. After some time, the transient magnetic diffusion process saturates, leading to a distribution of the magnetic induction that is no longer varying in time. At this time, the distribution of the magnetic induction exterior to the inclusion remains spatially nonuniform, but interior to the ellipsoid, the analysis outlined in Section 1.4 shows that the magnetic induction must be spatially uniform. A useful verification test then is to compare the configuration of the magnetic induction interior to the ellipsoid computed by ALEGRA to that predicted by the analysis.

To carry out this verification test, a series of simulations is designed for ALEGRA in 3-D. Dimensions and material properties including conductivity and permeability are chosen for the inclusion and the surrounding region, and an imposed magnetic field $H^{i\circ}$ is defined. Discretizations are then chosen to allow a convergence analysis by spatial refinement of the mesh. The simulations are set to

run sufficiently late in time to reach the equilibrium condition, and comparison to the analytic result is made at this time.

2.3 Sample Simulation Results

Results from a sample 3-D ALEGRA simulation are shown in Fig. 1. Here, an ellipsoid with a major/minor radius of 1.8/0.56 cm is modeled for an imposed magnetic induction of 1.0 T oriented in the *y*-direction (vertical in these images). The ellipsoid axis lies along the *z*-direction, and 60 mesh elements span the *z*-dimension of the ellipsoid. It has a conductivity of 10^7 S/m and a permeability exceeding the permeability of free space μ_0 by a factor of 3 (i.e., a relative permeability $\mu_- = 3$). The exterior region has a conductivity of 10^{-6} S/m and permeability equal to μ_0 (i.e., a relative permeability of 1). The magnetic induction B_i evolves over time until a steady state is reached and negligible current persists. At that time, the magnetic induction inside the ellipsoid is uniform, as predicted by the preceding analysis.

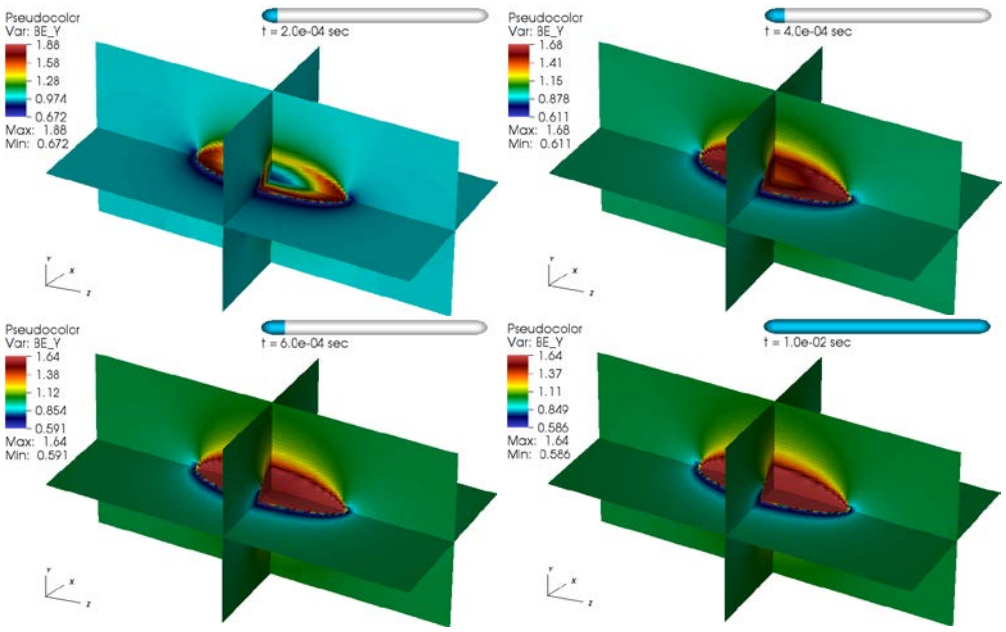

Fig. 1 Computed solutions for the vertical magnetic induction (B_y) from ALEGRA during and after equilibration. The analytic solution predicts 1.5788 T inside the ellipsoid.

Evaluating Eq. 34 for this geometry and imposed magnetic field predicts a vertical magnetic induction B_y inside the ellipsoid of 1.5788 T. In the simulation, the mean equilibrium interior field is approximately B_y = 1.596 T. Comparison with the analytic solution reveals that the approximation used to insert the ellipsoidal shape into the domain must be improved for precise comparison. Increasing the number of analytical points in the elliptical cross section when computing initial

element-wise volume fractions from 90 to 720 improves the computed result. The lateral extent of the simulation mesh also affects the accuracy of the result and must be a factor of 3 to 4 larger than the extent of the ellipsoid in any direction—only a subregion of the domain is shown in Fig. 1. Of course, the mesh resolution affects the accuracy as well, and this is explored in the following section.

The 3-D simulations shown in Fig. 1 are analogous to the 2-D ALEGRA simulations described in Refs. 5 and 6, in that the aspect ratio of the 2-D ellipse has been used here for a 3-D ellipsoid, and the orientation of the magnetic field, dimensions, and material properties are all the same. However, the physical time required to reach a steady-state condition is much smaller in this 3-D ellipsoid case than in the 2-D ellipse case. For the ellipse or elliptical cylinder case, roughly 2 ms is required for the rate of electromagnetic energy deposition in the mesh by the imposed magnetic field to drop by 3 orders of magnitude from its initial rate. In the 3-D ellipsoid case, only about 0.5 ms is required for the same drop. Magnetic diffusion proceeds to a steady state much more quickly for ellipsoid than for the elliptical cylinder of the same cross section.

2.4 Verification Analysis

To provide a rigorous verification test for ALEGRA in 3-D, a more challenging geometry than that shown in Fig. 1 is used here. The ellipsoid is elongated to an aspect ratio e = 10, and an oblique imposed magnetic field is used, given by $H^{i\circ} = \left(\mu_0\sqrt{3}\right)^{-1}(\hat{x}+\hat{y}+\hat{z})$ A/m. This geometry is shown schematically in Fig. 2.

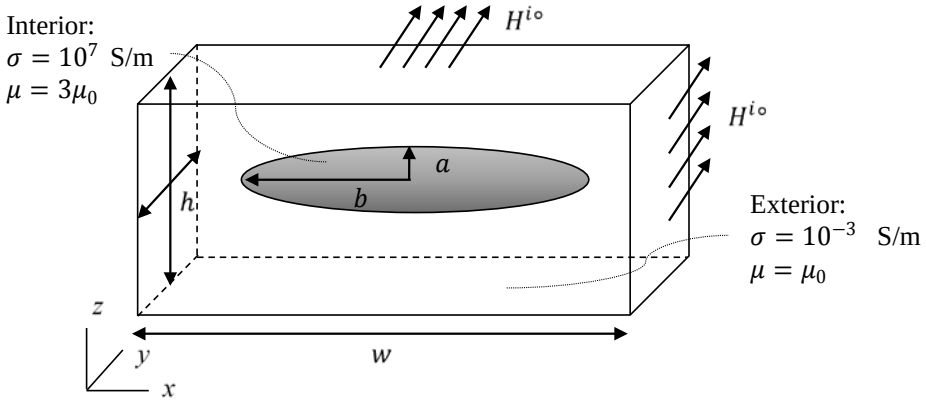

Fig. 2 Geometry for verification test in ALEGRA (not to scale)

The ellipsoid dimensions (semi-axes) for the verification problem are a = 3.16 cm in the x-direction and b = 0.316 cm in the y- and z-directions. Computational mesh dimensions are w = 24 cm in the axial (x) direction and h = 15 cm in the transverse (y and z) directions. Based on the outcome of the verification study in Refs. 5 and

6, only a regular rectangular mesh is used here, with no body-fitting. The mesh is composed of unit–aspect–ratio (cubic) hexahedral elements in the region of the ellipsoid, with gradually larger rectangular elements stretching out to the boundaries.

Convergence of the steady-state solution at t = 1.2 ms under spatial refinement is studied by simulating this geometry in ALEGRA with meshes ranging from N = 20 to N = 640 elements spanning the axial length of the ellipsoid. The exact solution predicted by Eq. 34 for the ellipsoid-interior magnetic induction in this system is $B_x = 1.6645184$ T and $B_y = B_z = 0.8748995$ T. Error estimates for these simulations are obtained by taking an L2 norm over all values of B_x, B_y, and B_z interior to the ellipsoid with respect to this uniform exact solution. A fractional error norm is then the ratio of this L2 error norm to the analytical value of the magnetic induction. This norm can be measured either with or without the transitional layer of mixed-material elements that span the void-material interface at the ellipsoid surface.

Measurements of the fractional L2 error in the solution for B_x with and without the mixed elements are shown in Fig. 3. We see that the error is dominated by the interfacial region where mixed-material elements are present. When the interfacial region is included (all nonexterior elements, or elements where ellipsoid material is present in any amount), the error magnitudes are larger by more than an order of magnitude, and the convergence rate drops from roughly 1 to roughly 0.5. Data for N = 20 without mixed-material elements are not included, because the N = 20 mesh is so coarse that all elements interior to the ellipsoid are mixed elements.

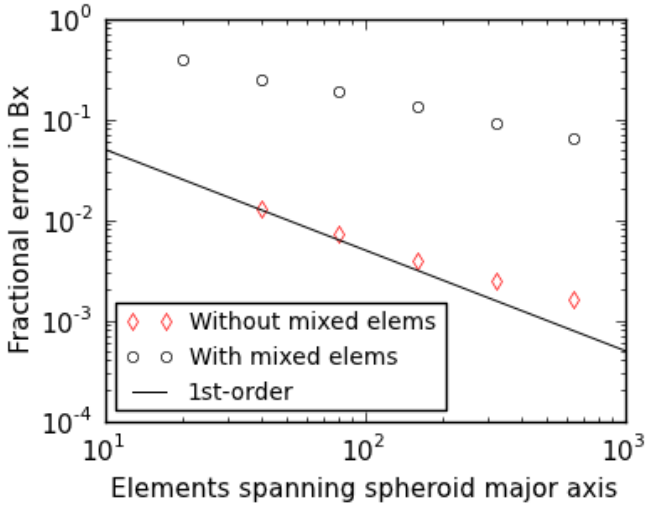

Fig. 3 Convergence behavior with and without the layer of mixed elements on the ellipsoid surface

Since this initial measurement demonstrates that the mixed-material elements in the simulation carry large errors, the analysis is repeated using successively smaller interior subregions of the ellipsoid, with lateral and axial dimensions 75% and 15% of the actual inclusion. The convergence trends for B_x and B_y in these subregions are shown in Fig. 4. The convergence trend for B_z is nearly identical to that for B_y, so it is not shown here.

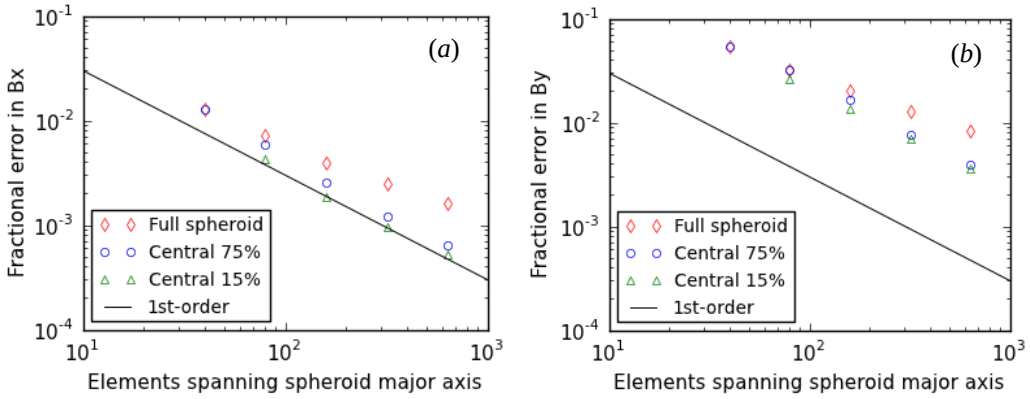

Fig. 4 Convergence trends for (*a*) the *x*-component and (*b*) the *y*-component of magnetic induction, for various subregions of the spheroid inclusion

The solution computed by ALEGRA converges monotonically at approximately first order to the predicted analytic solution. The convergence rate and error magnitudes improve as the ellipsoid sampling subregion shrinks, and fewer elements near the interface are included in the error sum. The error magnitudes are significantly smaller for B_x than for B_y and B_z, because of the major/minor axis asymmetry that has been built into this test. The convergence rates are shown in Table 1.

Table 1 Convergence rates for spheroid verification study for various subregions.

Case	Rate for B_x	Rate for B_y	Rate for B_z
All nonexterior elements	0.525	0.365	0.365
No mixed elements	0.755	0.675	0.675
Central 75%	0.864	0.759	0.759
Central 15%	1.013	0.961	0.961

2.5 Origin of Diminished Convergence Rates

Since verification is done here using magnetic induction *B* (of most interest to ALEGRA users), rather than the native vector potential *A*, we expect only first-order convergence of the solutions. This is because the magnetic induction is not the native finite-element solution variable, and ALEGRA must use certain approximations to obtain *B*. Thus, first-order convergence with respect to spatial

mesh refinement is what we expect, and that is what we observe in the tests, so long as the region near the material interface is excluded.

Further investigation into the origins of the larger error magnitudes and diminished convergence rates near the interface shows that anomalous spatial oscillations persist in the solution even at steady state. These are shown in Fig. 5 for the 3 finest mesh resolutions, where spatial distributions of the fractional difference between the computed and analytic values of B_x are plotted on a slice through the ellipsoid centroid normal to the *z*-direction. These oscillations also appear in the 2-D solutions discussed in Ref. 5 for the regular-mesh cases.

The oscillations are unphysical and arise because in the mixed-material elements, the natural interface conditions on *B* and *H* (see Eq. 3) are not enforced explicitly, since the interface is actually treated as a volumetrically mixed zone at the level of the Eulerian spatial discretization. Further, when an ALEGRA simulation includes materials with distinct magnetic permeabilities, the element-level homogenization scheme actually averages the reluctivity, not the permeability. Such prominent oscillations have not been observed in magnetic diffusion simulations where the magnetic permeability is μ_0 everywhere. Therefore, these results suggest that the option to form an average element permeability might be useful.

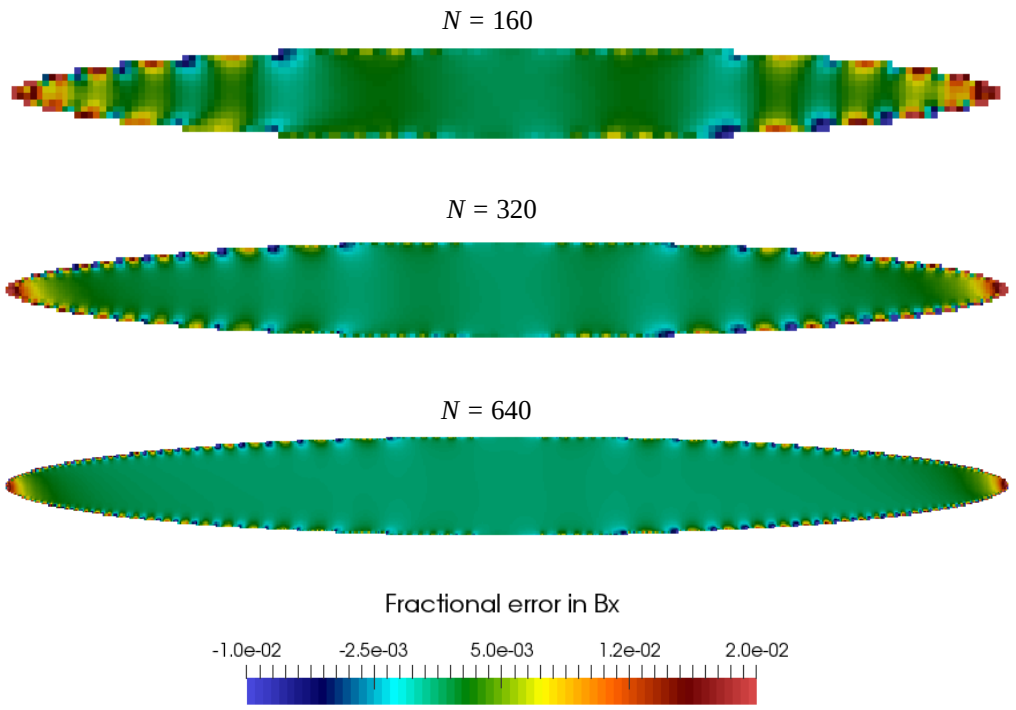

Fig. 5 Spatial distribution of error in ellipsoid-interior magnetic induction at steady state, arranged by increasing number of *N* elements spanning the axial length of the ellipsoid

2.6 Computational Cost

The ALEGRA simulations conducted here vary enormously in computational cost. At $N = 40$, the mesh has 16,800 elements, and the simulation runs to completion in a few minutes on 8 processors. At $N = 640$, the mesh has 56 million elements (1.7 billion edges) and runs to completion in about 3 days on 4,096 processors. This is very near the upper limit of the computational domain size that can be used in ALEGRA.

3. Conclusions

This work shows how the equilibrium/steady-state condition of the magnetic field in an ellipsoidal inclusion can be obtained analytically. The analysis results in a simple, elegant closed-form expression that describes a uniform magnetic field in the ellipsoid interior exactly. The expression is easily evaluated within verification testing techniques, making it well suited for use in verification of electromagnetics modeling tools like ALEGRA.

Convergence testing using this analytic solution shows that the equilibrium magnetized state can be reached by transient means via computation with ALEGRA. The solution in the interior core of the ellipsoid converges to the exact solution at first order, as expected, for a very large range of spatial mesh sizes spanning the very coarsest to the very finest meshes that are possible using ALEGRA.

The verification work reveals 2 significant issues in the computation of magnetic diffusion for magnetically permeable materials on Eulerian (nonbody-fitted) meshes. Those issues are 1) that the natural boundary conditions on B and H are not enforced explicitly and 2) that element-level homogenization of the elements on the ellipsoid interface using reluctivity can be inaccurate. These issues result in noticeable local perturbations from the exact uniform solution, which corrupt the ellipsoid interior field slightly and cause deterioration of the convergence rate when these elements are included in the error metric.

Verification testing is applied here by developing an analytic solution and using convergence analysis. The test results can be used to advance the algorithms in ALEGRA and codes like it. It is anticipated that future work extending those algorithms can make use of the analytic solution and results.

4. References

1. Knoepfel H. Pulsed high magnetic fields. 1st ed. Netherlands: North Holland Publishing Co.; 1970.
2. Rieben RN, White DA. Verification of high-order mixed finite-element solution of transient magnetic diffusion problems. IEEE Trans Mag. 2006; (42): 25–39.
3. Woodson HH, Melcher JR. Electromechanical dynamics. Hoboken (NJ): Wiley; 1968.
4. Brauer JR. Magnetic diffusion times for infusion and effusion in nonlinear steel slabs and cylinders. IEEE Trans Mag. 2007;4(2):3181–3188.
5. Grinfeld MJ, Niederhaus HJ, Porwitzky AJ. Assessment of ALEGRA computation for magnetostatic configurations. ACES Exp J. 2016;1(2):40–43.
6. Grinfeld M, Niederhaus J, Porwitzky A. Using the ALEGRA code for analysis of quasistatic magnetization of metals. Aberdeen Proving Ground (MD): Army Research Laboratory (US); 2015 Sep. Report No.: ARL-TR-7415.
7. Landau LD, Lifshitz EM. Electrodynamics of continuous media. Oxford (UK): Pergamon; 1984.
8. Jackson JD. Classical electrodynamics. Hoboken (NJ): Wiley; 1999.
9. Grinfeld MA. Thermodynamic methods in the theory of heterogeneous systems. Sussex (UK): Longman; 1991.
10. Eshelby JD. The determination of the elastic field of an ellipsoidal inclusion, and related problems. Proc Roy Soc A. 1957;241:376–396.
11. Eshelby JD. The elastic field outside an ellipsoidal inclusion. Proc Roy Soc A. 1959;252:561–569.
12. Kellogg OD. Foundations of potential theory. Berlin: Springer; 1929.
13. Robinson AC, Brunner TA, Carroll S, Drake R, Garasi CJ, Gardiner T, Haill T, Hanshaw H, Hensinger D, Labreche D, et al. ALEGRA: an arbitrary Lagrangian-Eulerian multimaterial, multiphysics code. Proceedings of the 46th AIAA Aerospace Sciences Meeting; Reno, NV; 2008 Jan 7–10.

List of Symbols, Abbreviations, and Acronyms

2-D	2-dimensional
3-D	3-dimensional
MHD	magnetohydrodynamics
PDE	partial differential equation
V&V	verification and validation

1 (PDF) DEFENSE TECHNICAL INFORMATION CTR DTIC OCA

2 (PDF) DIRECTOR USARL RDRL CIO L IMAL HRA MAIL & RECORDS MGMT

1 (PDF) GOVT PRINTG OFC A MALHOTRA

3 (PDF) USARL RDRL WMP A J CAZAMIAS RDRL WMP C M GRINFELD RDRL WMP D R DONEY

2 (PDF) SANDIA NTL LAB J NIEDERHAUS C SIEFERT